An electron acceptor featuring a B-N covalent bond and small singlet-triplet gap for organic solar cells

ChemComm

COMMUNICATION

View Article Online
View Journal | View Issue

Cite this: *Chem. Commun.*, 2022, **58**, 8686

Received 6th June 2022,
Accepted 4th July 2022

DOI: 10.1039/d2cc03172h

rsc.li/chemcomm

An electron acceptor featuring a B–N covalent bond and small singlet–triplet gap for organic solar cells†

Xinyuan Liu,‡[a] Shuting Pang,‡*[a] Liang Zeng,[a] Wanyuan Deng,[a] Mingqun Yang,[a] Xiyue Yuan,[a] Junyu Li,[b] Chunhui Duan, *[a] Fei Huang [a] and Yong Cao[a]

BNTT2F, an electron acceptor featuring a B–N covalent bond and singlet–triplet gap as low as 0.20 eV *via* the multiple resonance effect, is developed for organic solar cells. The optimized device based on BNTT2F offered an efficiency of 8.3%, suggesting the great prospect of B–N covalent bond-containing π-conjugated molecules for photovoltaics.

Organic solar cells (OSCs) have attracted much attention due to their advantages, including light weight, flexibility, roll-to-roll processability, *etc.*[1,2] In the past few years, the power conversion efficiencies (PCEs) of OSCs have been increased to 19%,[3,4] which mainly resulted from the progress in non-fullerene acceptors (NFAs).[5–8] Generally, high performance NFAs possess an acceptor–donor–acceptor (A–D–A) structure with an electron-donating (D) central core and two electron-withdrawing (A) end groups.[7–9] The optical absorption, photoluminescence quantum yield, and charge carrier mobility of NFAs could be finely tuned, which further affects the device performance of OSCs.

Heteroatom substitution is successful in tuning the physical and optoelectronic properties of organic semiconductors.[10–14] In particular, the incorporation of boron–nitrogen bonds into the conjugated skeleton is a new approach to tune the electronic structures of π-conjugated molecules and polymers.[15] Boron and nitrogen atoms can form two kinds of bond, *i.e.* a B←N coordinate bond and a B–N covalent bond.[15] B←N coordinate bonds have been used to construct both polymeric and small molecular NFAs.[16–19] Different from B←N coordinate bonds, the boron atom in B–N covalent bonds adopts sp^2 hybridization, which offers a coplanar conjugated skeleton that benefits ordered molecular packing and efficient charge transport.[20–22] For example, our group has recently reported a B–N covalent bond featured polymer PBNT-BDD for high-performance OSCs.[20] Moreover, the multiple resonance effect induced by boron and nitrogen atoms in conjugated molecules can lead to a small energy gap (ΔE_{ST}) between the singlet (S_1) and triplet (T_1),[14] which is desired to suppress the recombination *via* the triplet state in OSCs.[23–25] Previously, we have observed this property in a B–N covalent bond-based polymer donor.[20] However, the utilization of B–N covalent bonds in designing electron acceptors with small ΔE_{ST} for OSCs remains to be reported.

Herein, we report a novel A–D–A-type π-conjugated molecule featuring a B–N covalent bond for use as an electron acceptor in OSCs for the first time. The new acceptor BNTT2F possesses a B–N covalent bond-containing central core (BNTT) with excellent coplanarity and exhibits ΔE_{ST} as low as 0.2 eV. A promising PCE of 8.3% has been obtained in OSCs by blending BNTT2F with the polymer donor PM6, which suggests the great prospect of B–N covalent bond-containing π-conjugated molecules in OSCs.

The synthetic route of BNTT2F is shown in Scheme 1. The compound 2 was generated by the palladium-catalyzed Stille cross-coupling reaction starting from the compound 1. The subsequent cyclization gave the fused compound 3 (BNTT) in 80% yield using a boron reagent. The compound 3 was then oxidized with phosphorus oxychloride, and quenched with *N*,*N*-dimethylformamide to yield the aldehyde-containing compound 4. The Knoevenagel condensation between the compound 4 and 2-(5,6-difluoro-3-oxo-2,3-dihydro-1*H*-inden-1-ylidene)malono-nitrile afforded the target compound BNTT2F in 70% yield. The final product was fully characterized by ^{1}H and ^{13}C nuclear magnetic resonance (NMR) and matrix-assisted laser desorption ionization time-of-flight (MALDI-TOF) mass spectroscopy (MS) (see the ESI†). Notably, BNTT2F did not exhibit peak splitting in the ^{1}H NMR spectrum acquired at room temperature (Fig. S7, ESI†), suggesting its strong aggregation. The aggregation of BNTT2F can be inhibited by elevating

[a] *Institute of Polymer Optoelectronic Materials and Devices, State Key Laboratory of Luminescent Materials and Devices, South China University of Technology, Guangzhou, 510640, China. E-mail: pangshuting@scut.edu.cn, duanchunhui@scut.edu.cn*

[b] *Molecular Materials and Nanosystems & Institute for Complex Molecular Systems, Eindhoven University of Technology, MB Eindhoven, 5600, The Netherlands*

† Electronic supplementary information (ESI) available. See DOI: https://doi.org/10.1039/d2cc03172h

‡ These authors contributed equally to this work.

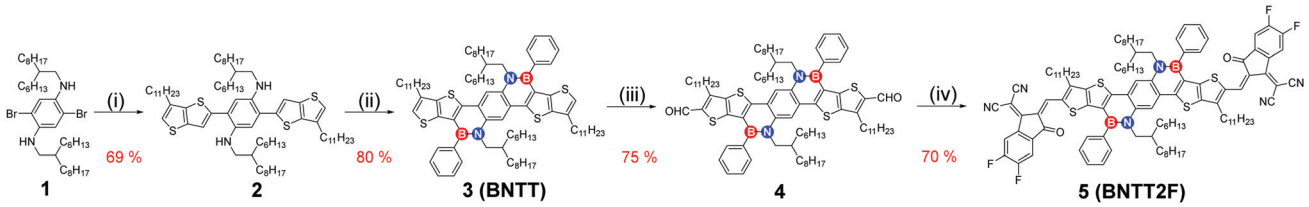

Scheme 1 The synthetic route of BNTT2F. (i) Tributyl(6-undecylthieno[3,2-*b*]thiophen-2-yl)stannane, $Pd(PPh_3)_4$, *o*-xylene, 120 °C; (ii) phenyl dichloroborane, triethylamine, *o*-dichlorobenzene, 180 °C; (iii) phosphorous oxychloride, 1,2-dichloroethane, dimethylformamide, 60 °C; (iv) 2-(5,6-difluoro-3-oxo-2,3-dihydro-1*H*-inden-1-ylidene)malono-nitrile, pyridine, chloroform, 65 °C.

the solution temperature, and the ^{1}H NMR spectrum with clear peak splitting was obtained at 100 °C (Fig. S8, ESI†). BNTT2F exhibits good solubility in common organic solvents, such as chloroform and chlorobenzene.

Thermal gravimetric analysis (TGA) suggested that the weight loss was lower than 5% until the temperature reached 321.1 °C (Fig. S11a, ESI†), indicating the good thermal stability of BNTT2F. The crystallization peak at 290.0 °C was observed from differential scanning calorimetry (DSC) analysis (Fig. S11b, ESI†), suggesting the strong crystallinity of BNTT2F. The absorption spectra of BNTT2F in dilute solution and thin films are shown in Fig. 1a. Going from solution to film, the absorption peak of BNTT2F was red-shifted from 636 to 673 nm. The absorption onset of the BNTT2F film was located at 732 nm, corresponding to an optical bandgap of 1.69 eV. The absorption spectrum of BNTT2F is complementary to that of the polymer donor PM6. The lowest unoccupied molecular orbital (LUMO) and highest occupied molecular orbital (HOMO) energy levels of BNTT2F determined by square wave voltammetry (SWV) were −4.07 and −6.00 eV (Fig. S12, ESI†), respectively. The deep-lying LUMO energy level indicates that BNTT2F can be used as an electron acceptor for OSCs. Moreover, the LUMO–LUMO and HOMO–HOMO offsets between PM6 and BNTT2F are large enough for efficient electron and hole transfer.[26,27]

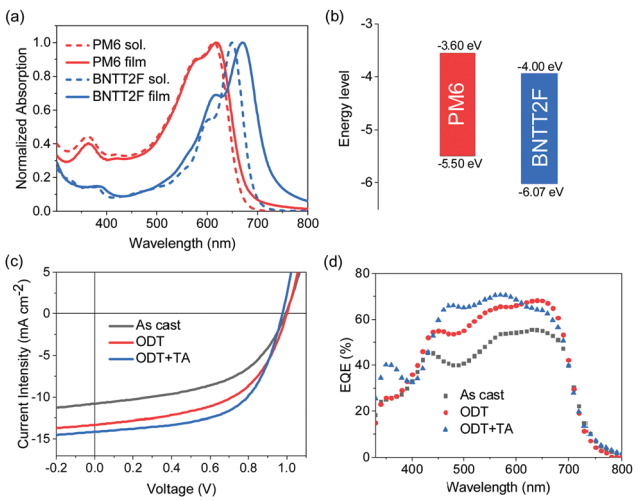

Fig. 1 (a) Absorption spectra and (b) energy levels of PM6 and BNTT2F; (c) *J*–*V* curves and (d) EQE spectra of the PM6:BNTT2F-based OSCs.

Density functional theory (DFT) calculations were performed to evaluate the molecular geometries, frontier orbital distributions, and energy levels. The conjugated skeleton of BNTT2F shows excellent coplanarity (Fig. S13a, ESI†), which is favourable for efficient intramolecular charge transfer (ICT) and compact intermolecular π–π stacking. The dihedral angle between the peripheral phenyl and molecular principal plane is 69.38°, which can prevent excessive aggregation. The HOMO is well delocalized along the central BNTT unit, while the LUMO involves a considerable contribution from the electron-withdrawing end groups (Fig. S13b, ESI†). The calculated LUMO and HOMO energy levels are −3.80 and −6.07 eV, indicating that BNTT2F can be used as an electron acceptor in OSCs.

The photovoltaic property of BNTT2F was evaluated in OSCs with a configuration of ITO/PEDOT:PSS/PM6:BNTT2F/PNDIT-F3N/Ag. It was found that solvent additive and thermal annealing (TA) can improve the device performance of OSCs (Table S1, ESI†). The current density–voltage (*J*–*V*) curves of the devices are shown in Fig. 1c, and the photovoltaic parameters are summarized in Table 1. The as cast device processed from chloroform afforded a PCE of 5.1% with a short circuit current density (J_{sc}) of 10.9 mA cm^{-2} and a fill factor (FF) of 47%. By introducing 0.25% (v/v) 1,8-octanedithiol (ODT) as a solvent additive, a higher PCE of 6.8% was obtained due to the improved J_{sc} (12.8 mA cm^{-2}) and FF (51%). Additional TA treatment further improved the PCE to 8.3% along with a J_{sc} of 13.8 mA cm^{-2} and an FF of 61%. The improvement in J_{sc} has been confirmed by the external quantum efficiencies (EQEs) of the OSCs (Fig. 1d). The devices with ODT and ODT + TA treatment exhibited higher EQEs in the spectral range from 430 to 680 nm with the maximum value of ≈70%. Notably, the OSCs of PM6:BNTT2F offered an open-circuit voltage (V_{oc}) of ≈1.00 V, which is considerably superior to the OSCs based on PM6:Y6 and PM6:IT-4F.[6,28]

The charge transfer behaviors of the blend films were explored *via* photoluminescence (PL) spectra (Fig. S14, ESI†). Compared with the PL spectra of the neat PM6 and BNTT2F films excited at 530 and 655 nm, respectively, all the PM6:BNTT2F blend films (as cast, ODT, and ODT + TA) showed high PL quenching efficiencies. The blend film with ODT + TA treatment exhibited the highest PL quenching efficiency for both the donor (98.8%) and the acceptor (89.2%). These results indicate that the photo-generated excitons can be dissociated into free charge carriers at the D–A interface efficiently.

Table 1 Photovoltaic parameters of the PM6:BNTT2F-based OSCs under AM1.5G irradiation (100 mW cm^{-2})[a]

Treatment	V_{oc} (V)	J_{sc} (mA cm^{-2})	J_{sc} (EQE_{cal})[b] (mA cm^{-2})	FF (%)	PCE (%)
As cast	1.00 (1.00 ± 0.01)	10.9 (10.5 ± 0.3)	10.4	47 (46 ± 1)	5.1 (4.9 ± 0.2)
ODT	1.00 (0.99 ± 0.01)	13.3 (13.2 ± 0.1)	12.8	51 (51 ± 0)	6.8 (6.6 ± 0.2)
ODT + TA	0.99 (0.99 ± 0.01)	13.8 (13.8 ± 0.2)	13.5	61 (61 ± 0)	8.3 (8.2 ± 0.1)

[a] The data in brackets are the average values and standard deviation of at least 16 independent devices for each blend. [b] The J_{sc} (EQE_{cal}) is obtained from the integration of the EQEs to the AM1.5G spectrum.

The hole (μ_h) and electron (μ_e) mobility of the PM6:BNTT2F blend films were measured *via* the space charge limited current (SCLC) method (Fig. S15 and S16, ESI†). The μ_h and μ_e were 0.7×10^{-4} and 1.3×10^{-4} cm^2 V^{-1} s^{-1} for the as cast film, which were increased to 3.9×10^{-4} and 5.8×10^{-4} cm^2 V^{-1} s^{-1} for the ODT-treated film. After ODT + TA treatment, the μ_h and μ_e were further improved up to 1.4×10^{-3} and 1.7×10^{-3} cm^2 V^{-1} s^{-1}, consistent with the highest J_{sc} and FF of the resulting OSCs.

The photocurrent density (J_{ph}) *versus* effective voltage (V_{eff}) curves were measured to investigate the exciton dissociation and recombination process in the devices (Fig. S17, ESI†). The exciton dissociation efficiency $P(E, T)$ was calculated to be 91.3%, 92.9%, and 96.7% for the as cast, ODT, and ODT + TA treated devices, respectively, indicating that both ODT and TA treatment can promote exciton dissociation.

The light intensity dependence of J_{sc} and V_{oc} was measured to explore the charge recombination in OSCs (Fig. S18, ESI†). The relationship between J_{sc} and incident light intensity (P_{light}) can be described as $J_{sc} \propto P_{light}^{\alpha}$.[29] The power-law factor α of the ODT + TA device is 0.973, which is higher than that of the as cast device (α = 0.904) and ODT device (α = 0.956) (Fig. S18a, ESI†). These results show that ODT and TA treatment can effectively reduce bimolecular recombination. The relationship between V_{oc} and P_{light} is given by $V_{oc} \propto (nkT/q)\ln(P_{light})$.[30] The as cast device offered an n value of 1.77, whereas the n value was reduced to 1.34 and 1.10 for ODT and ODT + TA devices, respectively (Fig. S18b, ESI†). The lowest n value suggests that trap-assisted and geminate recombination was suppressed in the ODT + TA device.

Transmission electron microscopy (TEM) was used to investigate the morphology of the PM6:BNTT2F blends (Fig. 2a). TEM images demonstrated that the PM6:BNTT2F blends became less phase separated and more homogeneous from the as cast film to the ODT and ODT + TA treated films. Moreover, fibrillary structures can be observed in the film with ODT + TA treatment, which is conducive to exciton diffusion and charge carrier transport.

The molecular packing and orientation in the films were studied by grazing-incidence wide-angle X-ray scattering (GIWAXS). As shown in Fig. S19a (ESI†), the neat BNTT2F film displayed a (010) diffraction peak at q = 1.73 $Å^{-1}$ in the out-of-plane (OOP) direction and (100) diffraction peak in the in-plane (IP) direction, indicating the formation of a predominant face-on orientation. The PM6:BNTT2F blend films also exhibited (010) scattering peaks at q = 1.73 $Å^{-1}$ in the OOP direction (Fig. 2b and Table S3, ESI†), suggesting that the preferential face-on orientation of BNTT2F was maintained. The crystal coherence length (CCL) of the OOP (010) diffraction is 17.67, 20.94, and 21.75 Å for the as cast, ODT and ODT + TA films, respectively. Similar enhancement in CCL of the IP (100) diffraction going from the as cast (74.55 Å) to ODT (82.54 Å) and ODT + TA (84.59 Å) films was also observed. The increased CCL suggests more ordered molecular packing, which supports the higher J_{sc} and FF in the resulting OSCs.

Recombination *via* the triplet state is a well-recognized loss pathway in OSCs, which can be inhibited by elevating the energy level of the triplet exciton ($E(T_1)$).[23–25] The research on thermally activated delayed fluorescence emitters has proved that the multiple resonance effect induced by the electron-deficient boron atoms and electron-rich nitrogen atoms can effectively separate the HOMO level and the LUMO level, and thus high $E(T_1)$ and small ΔE_{ST} can be realized in B–N covalent bond-containing organic semiconductors.[14] As shown in Fig. 3a, BNTT2F in dilute solution

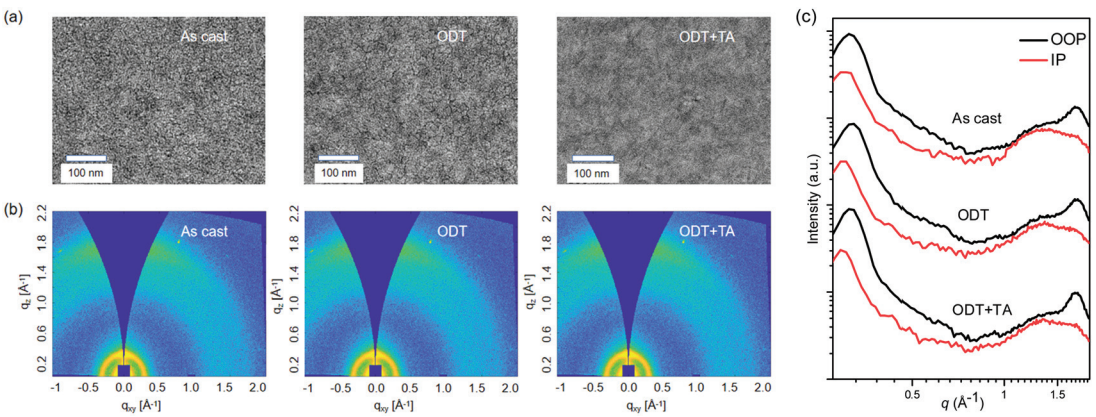

Fig. 2 (a) TEM images, (b) two-dimensional GIWAXS patterns, and (c) one-dimensional GIWAXS line-cut profiles of the PM6:BNTT2F blend films.

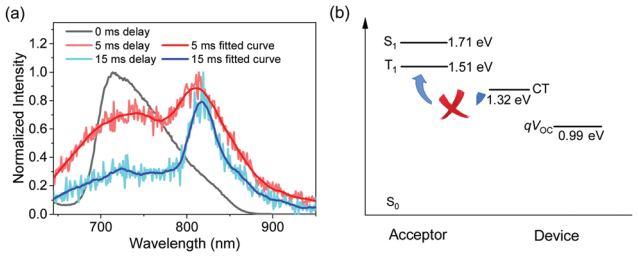

Fig. 3 (a) Fluorescent and phosphorescent emission spectra of the BNTT2F solution at 77 K with different delay times; (b) the Jablonski diagram of the electronic states in BNTT2F (ground state (S_0), singlet state (S_1), triplet state (T_1), charge transfer state (CT) and *V*oc of the OSCs).

at 77 K showed fluorescent and phosphorescent emission peaks at around 725 and 820 nm, corresponding to an energy level of 1.71 and 1.51 eV for the singlet and triplet, respectively. Correspondingly, the ΔE_{ST} of BNTT2F is as low as 0.20 eV, which is much lower than those of common organic semiconductors (0.6–1.0 eV). The energy level of the CT state (E(CT)) in PM6:BNTT2F solar cells was estimated to be 1.32 eV from the electroluminescence spectrum (Fig. S21, ESI†). Thus, the back transfer from the CT state to the triplet state of BNTT2F can be inhibited in principle (Fig. 3b).

In summary, a novel A–D–A type non-fullerene acceptor BNTT2F featuring a B–N covalent bond was developed. This is the first report on a B–N covalent bond-based electron acceptor for OSCs. BNTT2F exhibits a large coplanar backbone, intense optical absorption, and ideal energy levels. Favourable active morphology, efficient and balanced charge transport, and suppressed recombination losses were found for the optimized OSCs of PM6:BNTT2F after solvent additive and thermal annealing treatment. As a result, a decent PCE of 8.3% has been achieved by BNTT2F, which is also the highest one among the small molecular NFAs featuring either a B–N covalent bond or B←N coordinate bond. More importantly, BNTT2F possesses high $E(T_1)$ and small ΔE_{ST}, which would reduce recombination losses from the CT state to the triplet state theoretically. These results indicate that the introduction of a B–N covalent bond is an effective strategy to develop high-performance electron acceptors for OSCs.

The research was financially supported by the Ministry of Science and Technology of China (2019YFA0705900), National Natural Science Foundation of China (21875072, U20A6002, and 22109046), Guangdong Innovative and Entrepreneurial Research Team Program (2019ZT08L075), and Guangdong Basic and Applied Basic Research Foundation (2022A151-5011417). This work was also supported by the China Postdoctoral Science Foundation (2020TQ0102).

Conflicts of interest

There are no conflicts to declare.

Notes and references

1 G. Yu, J. Gao, J. C. Hummelen, F. Wudl and A. J. Heeger, *Science*, 1995, **270**, 1789.
2 Y. Li, G. Xu, C. Cui and Y. Li, *Adv. Energy Mater.*, 2018, **8**, 1701791.
3 L. Zhu, M. Zhang, J. Xu, C. Li, J. Yan, G. Zhou, W. Zhong, T. Hao, J. Song, X. Xue, Z. Zhou, R. Zeng, H. Zhu, C.-C. Chen, R. C. I. MacKenzie, Y. Zou, J. Nelson, Y. Zhang, Y. Sun and F. Liu, *Nat. Mater.*, 2022, **21**, 656.
4 Z. Zheng, J. Wang, P. Bi, J. Ren, Y. Wang, Y. Yang, X. Liu, S. Zhang and J. Hou, *Joule*, 2022, **6**, 171.
5 Y. Lin, J. Wang, Z.-G. Zhang, H. Bai, Y. Li, D. Zhu and X. Zhan, *Adv. Mater.*, 2015, **27**, 1170.
6 J. Yuan, Y. Zhang, L. Zhou, G. Zhang, H.-L. Yip, T.-K. Lau, X. Lu, C. Zhu, H. Peng, P. A. Johnson, M. Leclerc, Y. Cao, J. Ulanski, Y. Li and Y. Zou, *Joule*, 2019, **3**, 1140.
7 M. Yang, W. Wei, X. Zhou, Z. Wang and C. Duan, *Energy Mater.*, 2021, **1**, 100008.
8 C. Duan and L. Ding, *Sci. Bull.*, 2020, **65**, 1231.
9 X. Wan, C. Li, M. Zhang and Y. Chen, *Chem. Soc. Rev.*, 2020, **49**, 2828.
10 Z. Wang, Y. Shi, Y. Deng, Y. Han and Y. Geng, *Adv. Funct. Mater.*, 2021, **31**, 2104881.
11 B. Meng, Y. Ren, J. Liu, F. Jäkle and L. Wang, *Angew. Chem., Int. Ed.*, 2018, **57**, 2183.
12 X. Wang, H. Lin, T. Lei, D. Yang, F. Zhuang, J. Wang, S. Yuan and J. Pei, *Angew. Chem., Int. Ed.*, 2013, **52**, 3117.
13 S. Pang, M. Más-Montoya, M. Xiao, C. Duan, Z. Wang, X. Liu, R. A. J. Janssen, G. Yu, F. Huang and Y. Cao, *Chem. – Eur. J.*, 2019, **25**, 564.
14 T. Hatakeyama, K. Shiren, K. Nakajima, S. Nomura, S. Nakatsuka, K. Kinoshita, J. Ni, Y. Ono and T. Ikuta, *Adv. Mater.*, 2016, **28**, 2777.
15 J. Miao, Y. Wang, J. Liu and L. Wang, *Chem. Soc. Rev.*, 2022, **51**, 153.
16 C. Dou, X. Long, Z. Ding, Z. Xie, J. Liu and L. Wang, *Angew. Chem., Int. Ed.*, 2016, **55**, 1436.
17 C. Duan, G. Zango, M. G. Iglesias, F. J. M. Colberts, M. M. Wienk, M. V. Martínez-Díaz, R. A. J. Janssen and T. Torres, *Angew. Chem., Int. Ed.*, 2017, **56**, 148.
18 Y. Li, H. Meng, T. Liu, Y. Xiao, Z. Tang, B. Pang, Y. Li, Y. Xiang, G. Zhang, X. Lu, G. Yu, H. Yan, C. Zhan, J. Huang and J. Yao, *Adv. Mater.*, 2019, **31**, 1904585.
19 F. Liu, Z. Ding, J. Liu and L. Wang, *Chem. Commun.*, 2017, **53**, 12213.
20 S. Pang, Z. Wang, X. Yuan, L. Pan, W. Deng, H. Tang, H. Wu, S. Chen, C. Duan, F. Huang and Y. Cao, *Angew. Chem., Int. Ed.*, 2021, **60**, 8813.
21 P. Zhang, J. Zeng, F. Zhuang, K. Zhao, Z. Sun, Z.-F. Yao, Y. Lu, X. Wang, J. Wang and J. Pei, *Angew. Chem., Int. Ed.*, 2021, **60**, 23313.
22 W. Li, C. Du, X. Chen, L. Fu, R. Gao, Z. Yao, J. Wang, W. Hu, J. Pei and X. Wang, *Angew. Chem., Int. Ed.*, 2022, e202201464.
23 D. Veldman, S. C. J. Meskers and R. A. J. Janssen, *Adv. Funct. Mater.*, 2009, **19**, 1939.
24 A. Rao, P. C. Y. Chow, S. Gelinas, C. W. Schlenker, C.-Z. Li, H. L. Yip, A. K. Y. Jen, D. S. Ginger and R. H. Friend, *Nature*, 2013, **500**, 435.
25 A. J. Gillett, A. Privitera, R. Dilmurat, A. Karki, D. Qian, A. Pershin, G. Londi, W. K. Myers, J. Lee, J. Yuan, S.-J. Ko, M. K. Riede, F. Gao, G. C. Bazan, A. Rao, T.-Q. Nguyen, D. Beljonne and R. H. Friend, *Nature*, 2021, **597**, 666.
26 J. Liu, S. Chen, D. Qian, B. Gautam, G. Yang, J. Zhao, J. Bergqvist, F. Zhang, W. Ma, H. Ade, O. Inganäs, K. Gundogdu, F. Gao and H. Yan, *Nat. Energy*, 2016, **1**, 16089.
27 S. Chen, Y. Wang, L. Zhang, J. Zhao, Y. Chen, D. Zhu, H. Yao, G. Zhang, W. Ma, R. H. Friend, P. C. Y. Chow, F. Gao and H. Yan, *Adv. Mater.*, 2018, **30**, 1804215.
28 W. Li, L. Ye, S. Li, H. Yao, H. Ade and J. Hou, *Adv. Mater.*, 2018, **30**, 1707170.
29 S. R. Cowan, A. Roy and A. J. Heeger, *Phys. Rev. B: Condens. Matter Mater. Phys.*, 2010, **82**, 245207.
30 L. J. A. Koster, V. D. Mihailetchi, R. Ramaker and P. W. M. Blom, *Appl. Phys. Lett.*, 2005, **86**, 123509.